DYNAMIC BEHAVIOR OF NONCOHESIVE EMBANKMENT MODELS

by Jorge I. Bustamante [1]

Abstract

The results of testing seven embankment models of noncohesive material as well as results from an analog computation are presented. Three points are emphasized: 1) the unestable equilibrium of embankments with slope inclinations larger than the angle of repose; 2) similitude requirements as inferred from comparison among models in all respects alike but of different linear dimentions (60cm and 100cm in height); 3) agreement of a simplified analog simulation with the behavior of physical models when unestable equilibrium does not set in.

Nomenclature

a = width of the crown of the models;

B = intersection point of the slope and the crown plane at the middle section (z=2.23m);

C_c = coefficient of curvature: $C_c=(D_{30})^2/(D_{10}\cdot D_{60})$;

C_u = coefficient of uniformity: $C_u=D_{60}/D_{10}$;

D_P = limit size of grains such that P percent of the sample have size smaller than D_P, (P=10,30,60);

e = void ratio;

g = acceleration of gravity;

h = height of the embankment models;

l = length of a slope;

m_i = mass of the ith wedge;

P_i = resultant force normal to the lower ith wedge plane;

$\bar{p}$ = normal pressure on a slide plane;

R = ratio of vertical displacements in models 100-cm tall to those in models 60-cm tall; the R refers to both physical and analytical models;

s = shear resistance on a plane;

1. Research Professor, Inst. of Eng., Natl. Univ. of Mexico, Mexico, D.F.

T_N = damped period of the horizontal excitation applied to model N (N=15,16,...,21);

T_{60} = damped period of the horizontal excitation applied to a model 60-cm tall;

T_{100} = damped period of the horizontal excitation applied to a model 100-cm tall;

$\ddot{v}$ = vertical component of the acceleration of the shaking table;

$\ddot{v}_o$ = maximum vertical acceleration measured close to the first half cycle of longitudinal acceleration;

x_o = maximum measured (LVDT) displacement of the shaking table in the longitudinal direction; also maximum computed displacement: $x_o = \ddot{x}_o / \omega_1^2$;

$\ddot{x}$ = horizontal longitudinal component of the shaking table acceleration;

$\dot{x}_o$ = estimated maximum velocity of excitation: $\dot{x}_o = \ddot{x}_o / \omega_1$;

$\ddot{x}_o$ = amplitude of the shaking table acceleration measured at the first half cycle;

$\dot{y}_i$ = velocity of the ith wedge in direction parallel to its lower plane;

$\ddot{y}_i$ = acceleration of the ith wedge in direction parallel to its lower plane;

z = transversal coordinate axis on the table reference system. It is parallel to the crown axis; z = 2.23m corresponds to the middle section of a model;

Θ_i = angle between the lower plane of the ith wedge and a horizontal plane;

μ_i = coefficient of Coulomb friction between the ith wedge and the $(i-1)$th wedge

$$\mu_i = \begin{cases} \tan \phi_s \text{ if } \dot{y}_i - \dot{y}_{i-1} \cos(\Theta_i - \Theta_{i-1}) > 0 \\ -\tan \phi_s \text{ if } \dot{y}_i - \dot{y}_{i-1} \cos(\Theta_i - \Theta_{i-1}) < 0 \end{cases} ;$$

$$\mu_i \leq \tan \phi_s \text{ if } \dot{y}_i - \dot{y}_{i-1} \cos(\Theta_i - \Theta_{i-1}) = 0 ;$$

ϕ = angle of internal friction;

ω_1 = damped circular frequency of the longitudinal vibration

of the shaking table.

Introduction

Study of the dynamic behavior of rock embankments such as rock fill dams has mostly rested on the use of models due to the lack of an adequate theory regarding granular behavior. The use of models in itself does not usually permit extrapolation to prototypes, due to scale effects. However, a rational theory verified by model behavior will allow dealing with prototypes by applying the theory with the parameters that characterize the prototype. This is the approach presented in this study.

The testing program had as objectives: 1) to visualize the mechanism of the model deformation so as to permit the proposal of a numerical method; 2) to study the similitude requirements; and 3) to evaluate the influence of the slope inclination on behavior.

The void ratio was planned to equal the smallest that could be attained in the models. This avoids compaction effects that could obssure the behavior.

Mechanical properties of the Sand

Most of the sand used, whose mechanical properties are described subsequently, passed mesh No. 4 (4.76mm) and was retained in No. 8 (2.38mm). It was obtained at the Santa Fe mines in Mexico's Federal District; it was subangular, uniform, of volcanic origin, and containing large grain sizes. The selection was based on the reproducibility of grain distribution that can be attained with a uniform grain size; also on the fact that the change in void ratio has important bearing on the shearing strength for small void ratios and less so for high void ratios. The grains were selected large tending to minimize the influence of grain size on shearing strength.

The grain-size distribution is summarized as follows: D_{10}=3.03mm; D_{30} = 3.55mm; D_{60} = 4.21mm; C_u = 1.39; and C_c = 0.99.

Water contents, determined for control of every model, were smaller than 0.66 percent. The average specific gravity was 2.62.

Direct shear tests with confining pressures of a few grams per square centimeter, as required for model studies, were performed in a special plexiglass shear box (1). The void ratio was regulated by weighing the sand before placing it in the box. The controlled strain rate was 0.13 mm/min.

The shearing stress was computed dividing the load applied to the shear box by the corrected transversal area. Correction was made according to the relative displacement between the upper and lower parts of the shearing device. Results of these tests for

different normal pressures are shown in Fig. 1. These plots serve to infer the change in the effective angle of internal friction as a function of shearing deformation.

The angle of repose was determined by carefully building up a pile of sand up to 80cm in height. The mean value for six different heights was 34.5°. There was, however, a clear tendency for the angle of repose to become smaller when the height increased.

Construction of Embankment Models

All the models tested were of trapezoid section. The lateral wood forms used to hold the sand in the desired shape were placed as construction proceeded. This permitted building the models by layers and controlling the uniformity of their void ratio throughout the height. Before starting the construction of any model, the weight of sand and the number of tamping strikes per unit area were computed for every layer. The minimum void ratio ($e = 0.86$) obtained by this procedure and the number of standard strikes were determined at the beginning of the investigation.

The 4.5 x 4.5m shaking table used for the dynamic tests has transparent plexiglass walls along both its longitudinal sides. Thus, changes in the cross sections adjacent to these walls may be observed. Before starting construction, a thin film of Palma Christi oil was applied to the transparent walls and subsequently thin cellophane paper were placed over the oil. This reduced the constraining effect of the plexiglass on the model.

The models were dynamically excited by giving the shaking table an initial displacement and releasing it suddenly. The ensuing motion resembles a damped cosine. The amount of damping is of the order of 5 to 7 percent. The amplitude of displacement depends on the position of the table spring and on the planned acceleration. The force required was measured with a calibrated cylinder. It was computed multiplying the total mass of the shaking table and model by the intended acceleration.

When the system came to rest the central profile was measured. Internal changes, as observed through the plexiglass walls, were recorded. The maximum acceleration associated with successive shocks was augmented by small increments, until attaining 0.9g. The dynamic history of loading was varied somewhat from model to model; a large change was introduced in the test of model 21. The amplitudes of base acceleration for all the tests are given in Figs. 5 to 7. Average periods of longitudinal table motion are also shown, identified as T with a subscript.

The order of testing was selected at random, except for models

19, 20 and 21. Model 19 was obtained from model 15, after testing which, the loose sand was removed and the remainer was carved in from the surface, until a model resulted similar to 15 but with a height of 60cm. Due to a faulty operation of the starting system, the shaking table was set in motion with an unknown initial acceleration, of about 220 cm/sec^2, which produced considerable movement of particles. This excitation is referred to as shock motion 0 of model 19 in Fig. 5.

Models 20 and 21 were not originally planned. Model 21 was obtained from the part of the model 20 that did not suffer appreciable permanent deformation. Both models were similar in geometry.

A summary of the characteristics of the models tested is given in Table 1.

Accelerations Measured in the Models

With the transducers available, which can give relative errors among themselves of the order of 10 or perhaps 20 percent, no differences in the maximum longitudinal accelerations could be detected between the base and points up to 75 percent of the model height. The amplitude of transverse accelerations was practically nil while the vertical ones acquired transient values that were as large as 100 percent of the longitudinal accelerations. The main frequency of vertical accelerations was also large, so their effects on stability can well be neglected as verified under analog simulation.

Stability of Slopes

The slopes will be called either stable or unstable. By stable will be understood those slopes which, under horizontal accelerations of the order of gravity, will present small changes in geometry (displacement). In them any change in profile is produced by additional loads regardless of the shearing deformations. The unstable slopes are those which suffer large changes in geometry (failure) with no load increase or with a very small one after enough shearing deformation has taken place.

There were two types of unstable slopes according to the mode of failure. One was the progressive type, which started with a localized motion of particles, the motion propagating upwards and sideways throughout the entire slope. This type of failure, which has been observed during static tilting tests, represents a case of a soil structure instability triggered by the unlocking of some surface grains. The failure is conditioned by the granular structure and by the slope angle. Every grain plays a part in the process and no wedge type of motion takes place, at least if the acceleration is increased gradually up to failure. This type of behavior was observed in models 15 and 16 (Table 1) where the slope inclination is about 8 degrees larger than the angle of repose. The change in geometry of model 16 up to

shock motion 5 is shown in Fig. 2.

The second type of failure was observed by means of a slow motion camera. It is characterized by a wedge of material, which comprises the entire talus (4.5m long), moving as a unit, followed by a volume increase due to shearing and to the splitting of the wedge into individual particles that fall down until a new plane of stable equilibrium is attained (Fig. 3). This failure was contemplated in models 17 and 18. The slope inclination was 36.9°, which is about 2° larger than the angle of repose. In each one of these models two table motions of the same acceleration were required to produce the failure described. The phenomenon can be understood by looking at the stress-strain curve of the granular material (Fig. 1) which shows that after passing the peak strength, the resistance of the sand decreases. Therefore, even after the table acceleration is zero there can be particle motion if the slope inclination exceeds the reduced angle of internal friction.

The above discussion establishes that this type of dynamic failure of noncohesive embankments will be conditioned by two chief variables: the initial factor of safety against failure under gravity loads and the extent of sliding in the zone of shear displacement, which is related to the frequency of excitation. The duration of the dynamic disturbance in itself is unimportant; what matters is the amount of relative displacement induced in relation with that involved in strength reduction. If the reduced strength suffices to resist the gravity loads, there will be no important motion once the dynamic disturbance has ceased; otherwise failure will surely take place.

Since the granular material is unable to resist tension, the surface shearing strain increases monotonically so that eventually it will have a resistance equal to the minimum shearing strength of the material. Accordingly, the only stable slopes will be those constructed with the inclination not exceeding the angle of repose, which is a lower bound to the angle of internal friction.

In order to verify this last contention models 20 and 21 were built having slopes smaller than the 34.5° angle of repose; the angles were 33° in one side and 24.1° in the other. No sign of failure could be detected throughout the tests. There were only increments of displacement in each shock according to the accelerations imposed. Fig. 4 ilustrates this point.

Similitude Requirements

Dynamic similarity can be verified by comparing the vertical displacements on the models of 1.00m in height with those on the 0.60m models. Both have the same angle of internal friction and similarity in geometry. Hence, the usual assumption that the acceleration of gravity is an important parameter (2,3) leads to the conclusion that,

if the periods of excitation (as all time variables) follow the relationship $T_{100} = T_{60}\sqrt{100/60} = 1.29\ T_{60}$ (here T_{100} = period of ground excitation for the models 100-cm tall and T_{60} = period of ground excitation for the smaller models), then the vertical displacement of the larger model should be 1.67 times that of its smaller companion. To verify these requirements the 1.00-m models were shaken with periods of 1.20 to 1.24 times the corresponding period for the 0.60-m models. The vertical displacements obtained are depicted in Figs. 5 to 7 where also their ratio is shown. For the first shocks the ratios are large, no doubt because the smaller models (those subjected to higher-frequency excitations) start moving at higher acceleration levels than the larger models. However, when the number of shocks increases, displacements tend to maintain a ratio which is equal to the ratio of the periods of excitation. This suggest that the important variable to be considered in the similitude is not the table acceleration but its velocity. This contention although not fully established by the test, due, among other things, to variations in the loading history, is further supported by the analog simulation. In any event the importance of this finding justifies further study. If the velocity is the important parameter, the similitude requirements may entail, for a constant ratio of lengths between model and prototype, time ratios equal to the length ratios and different accelerations between model and prototype. Accordingly, models should be built of materials having a specific gravity different from that of the prototype.

Analog Simulation

The use of colored sand in the 30cm closer to the transparent plexiglass walls led to the conclusion that permanent displacements take place only at the inclined exterior surfaces and in a narrow region close thereto. The width of this region depends on the acceleration applied. It was also seen that the sand moves more the closer it is to the surface. It was also concluded that the lateral walls offered a restraint to the model motion. The maximum vertical displacement difference between the middle and the end sections was of the order of 25 percent. Nevertheless, the general shapes of the deformal profiles were the same. Qualitatively, therefore, the internal distortion can be inferred from the data gathered at the plexiglass walls. Accordingly it is justified to incorporate the observed mechanism of motion in the analytical model.

On the basis of the observed process of failure, of the type that involves wedge displacements, the analytical model having rigid wedges, as shown in Fig. 9, seems justified. A similar model has been proposed previously and it has been shown that, in a homogeneous embankment, if the surfaces of failure are plane, they must all pass through the toe (4). Good correlation has been found with experiments for the acceleration required to initiate sliding assuming a surface of failure that consists of two planes, one of them through the toe (5). Fig.

9 also shows the general equations, boundary conditions, and nature of the nonlinearities involved in the problem.

The nonlinear system of equations of the analytic approach were integrated using an analog computer. Simulation of the different models tested was performed assuming that the maximum dry friction that can develop between the rigid wedges is constant during the motion and equals the tangent of the mean angle of failure obtained from tilting tests of embankment models similar in geometry to the ones tested dynamically and with the same void ratio. The confidence interval for this angle was $47.2^{\circ} \pm 1.3^{\circ}$. The coefficient of friction assumed was 1.09.

It was also assumed that the deformations were of such order that the coefficients in the equations of motion did not change significatively. The horizontal and vertical excitations were assumed to be cosine functions of time with the frequency determined during testing. Three percent of critical was assumed for the degree of viscous damping. The amplitude of the vertical component of acceleration was taken as 50 percent the value of the horizontal component, except that when the latter was 0.80g or 0.90g the vertical acceleration was 0.60g. The frequency of vertical motion was taken as 25 cps in all cases, which amounts to three to four times the horizontal frequency.

Results of Analog Simulation

The results from the analog simulation were compared with those from model tests using as reference the vertical distance that the crown has descended, measured at the intersection between it and the steeper slope.

Both values are shown for models 18 and 20 in Figs. 11 and 12 where the maximum accelerations, velocities, and displacements estimated or measured are shown also. In these figures ω_1 represents the circular frequency of the shaking table. Three wedges were considered for the simulation with subtended angles of 1°, 2°, and 3°. The smallest angle corresponds to the outermost wedge, the largest one to the innermost one (Fig. 10). This selection is in accord with model observations. At the outset, when the surficial sand has sheared through only a small distance, the simulation predicts larger displacements than those which were measured. (This difference shows a dynamic resistance greater than that determined from the static tests. It is likely that the static tests provide a lower bound to the dynamic strength; this is not so much due to strain rate effects or to surface conditions, which were the same in both tests, but to differences in the mechanism of failure.) As soon as the shearing displacement of the sand wedge reaches a value of the order of 1cm (shock 11, model 20, Fig. 12, for example), the rate of increase of the displacement of the model exceeds that in the simulation. The same phenomenon is observed in the simulation of all the models. If one continues the comparison

further, the analog simulation again will give values appreciably greater than those observed in the models. This is no doubt due to the complete change in geometry that takes place in the physical models. Model 21 for instance will have a slope angle of about 25° instead of the original 33°. For design purpose this source of nonlinearity may not be important since design would hardly be based on a 10 percent reduction of the embankment height. The discrepancies observed for model 18, shocks 10 and 11 correspond to the wedge motion that ended up with the failure into individual particles (Fig. 3). This type of failure is not incorporated in the simulation.

In Fig. 10 are compared two profiles of model 20 with those obtained from the simulation. The lower profile in the figure shows the analog results. These profiles closely resemble those of the model.

To gage further the simulation effectiveness, the ratio of the computations of models 20 and 21, which had different frequencies of excitation, are compared in Fig. 7 with the ratios obtained from the measurements made on the models. The effect observed experimentally is correctly predicted, namely that for the range of frequencies involved the ratios of the vertical displacements are inversely proportional to the ratios of the frequencies of excitation. One may question the validity of this comparison, as it is based on the principle that the displacements in both models will be proportional at any stage of deformation. This relationship was observed to hold with adequate accuracy for the different angles and conditions of the three large models tested and of their four 60-cm companions.

Admitting that the simulation was at least qualitatively correct, some runs were made changing the phase angle of the vertical excitation as well as the amplitude. The values of the displacements were not significantly changed for a vertical frequency of the order of 25 cps or larger. For smaller frequencies the history of displacements will undoubtedly be different.

Conclusions

The investigation reported supports certain conclusions applicable to well compacted models and prototypes:

1. Embankment models constructed with slope angles exceeding the angle of repose of the granular material can withstand large accelerations. However, after some moderate shearing displacement (of the order of the larger grain sizes) the shearing strength is markedly reduced and a failure, even under moderate or nil accelerations, can ensue.

2. For slope angles equal to or smaller than the angle of repose no major failure occurs even after large shearing deformations. Each

shock will produce only increments of displacement, which depend on the kinetic energy involved.

3. Relative permanent displacements of particles are largest at the surface and decrease rapidly with depth. (This conclusion is based on the use of colored materials and their subsequent examination.) The interior granular material does not suffer permanent relative displacements. The superficial displacements can be assimilated to the motion of triangular wedges whose apexes are relatively close to the toe.

4. The comparative behavior of models 0.60 and 1.00m in height does not agree with elementary considerations, which ask for equal accelerations in the model and prototype to satisfy dynamic similarity. Deformations observed in the 0.60-models and in the 1.00-models show that the behavior calls for equality of velocities for proper dynamic similarity.

5. The analog simulation proposed, although much simplified, retains the principal features observed in the physical models. A more elaborate simulation with a larger number of wedges, in which the sand strength could be changed as a function of the total displacements of the wedges, and in which the change in geometry would be included, should anticipate accurately the model deformations. With proper strength parameters to take into consideration the nonlinearity of the Mohr-Coulomb strength envelopes for large pressures it could be applied to the prediction of prototype behavior, save for effects of large volume changes caused by crushing at points of contact between individual particles. The latter phenomenon has apparently received no consideration in relation to dynamic behavior and may be of paramount importance when the prototype particles are large fragments of rock.

Acknowledgment

This study was done at the Institute of Engineering of the National University of Mexico under sponsorship of the Federal Electricity Commission of Mexico. The writer is indebted to Emilio Rosenblueth, Director of the Institute, for his interest and critical revision of the manuscript. He is also grateful to Professors Nathan M. Newmark, Arthur Casagrande and Don U. Deere for their valuable suggestions during the development of the investigation. The material presented here is based upon a dissertation submitted in partial fulfillment of the requirements for the doctoral degree at the University of Illinois.

References

1. Bustamante, J. I., "Dynamic Behavior of Non-Cohesive Embankment Models," Ph.D. Thesis, University of Illinois (1964).

2. Clough, R. W., and Pirtz, D., "Earthquake Resistance of Rock-Fill Dams," Transactions of the American Society of Civil Engineers, Vol. 123 (1958), pp. 792-810.

3. Seed, H. B., and Clough, R.W., "Earthquake Resistance of Sloping Core Dams," Proceedings of the American Society of Civil Engineers, Vol. 89, No. SM1 (1963), pp. 209-242.

4. Rosenblueth, E., Appendix in the report by N. M. Newmark, "The Earthquakes Resistance of Portage Mountain Dam," Report to International Power and Engineering Consultants Limited (1960).

5. Goodman, R.E., "The Stability of Slopes in Cohesionless Materials during Earthquakes," Ph. D. Thesis, University of California, Berkeley (1963).

TABLE 1

ACTUAL CHARACTERISTICS OF THE DYNAMIC MODELS TESTED

MODEL NUMBER	AVERAGE HEIGHT h (meters)	AVERAGE VOID RATIO	SLOPE ANGLE SPRING SIDE [2]	SLOPE ANGLE STARTER SIDE	AVERAGE WIDTH OF THE CROWN	LENGTH OF MODEL l (meters)	ORDER THEY WERE TESTED
15	0.599	0.858	42.1°	36.5°	0.060	4.46	5
16	0.998	0.866	42.5°	37.0°	0.104	4.46	3
17	0.599	0.873	36.7°	24.0°	0.054	4.46	2
18	1.002	0.855	36.8°	24.0°	0.097	4.46	1
19	0.604	0.866	42.0°	37.4°	0.068	4.46	4
20	0.992	0.873	32.8°	23.6°	0.094	4.46	6
21	0.612	0.873	33.7°	24.3°	0.069	4.46	7

2. THIS SLOPE IS ON THE SIDE TOWARDS WHICH THE INITIAL ACCELERATION IS DIRECTED.

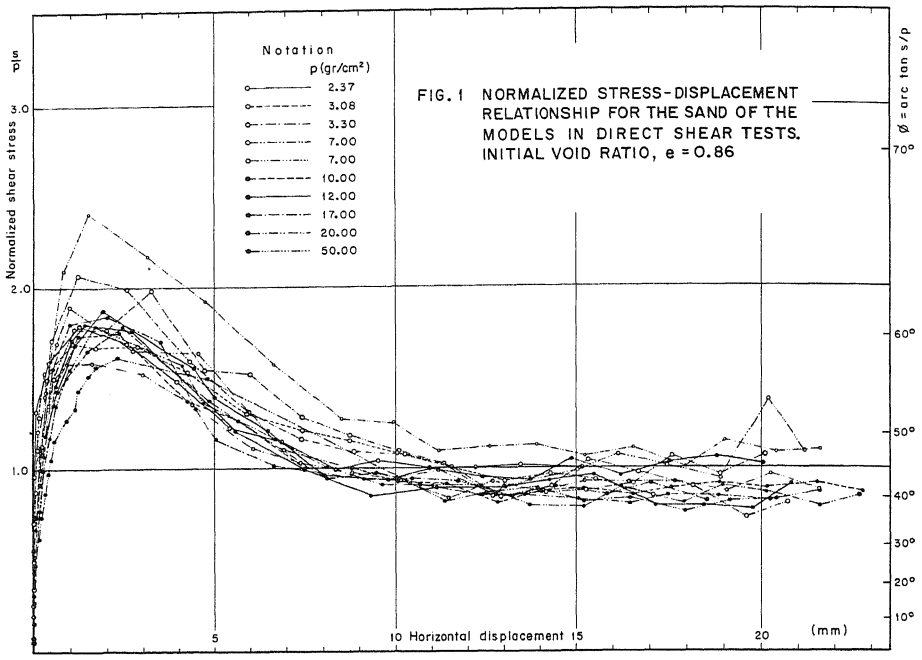

FIG. 1 NORMALIZED STRESS-DISPLACEMENT RELATIONSHIP FOR THE SAND OF THE MODELS IN DIRECT SHEAR TESTS. INITIAL VOID RATIO, e = 0.86

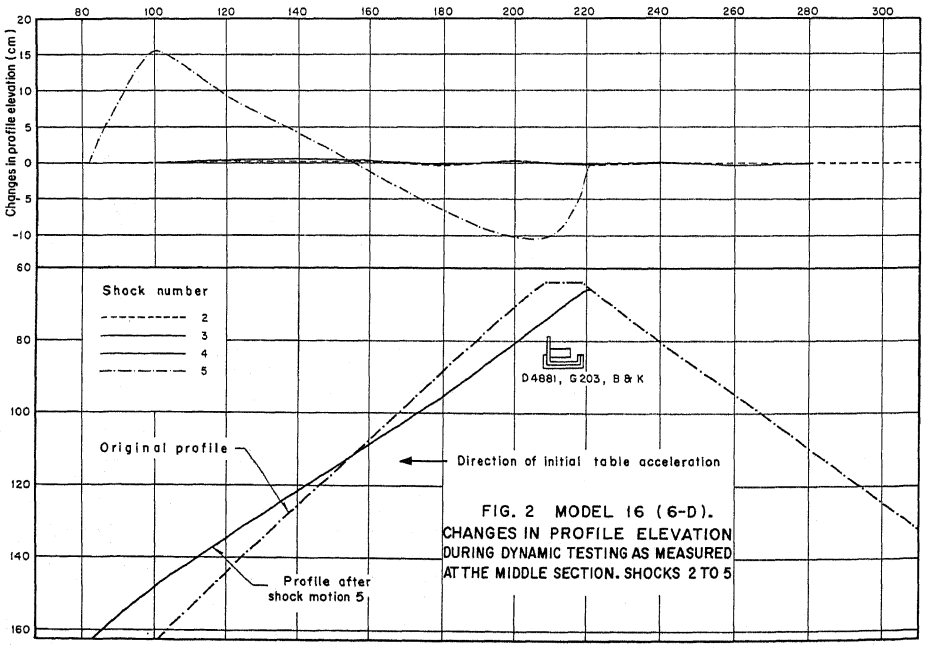

FIG. 2 MODEL 16 (6-D). CHANGES IN PROFILE ELEVATION DURING DYNAMIC TESTING AS MEASURED AT THE MIDDLE SECTION. SHOCKS 2 TO 5

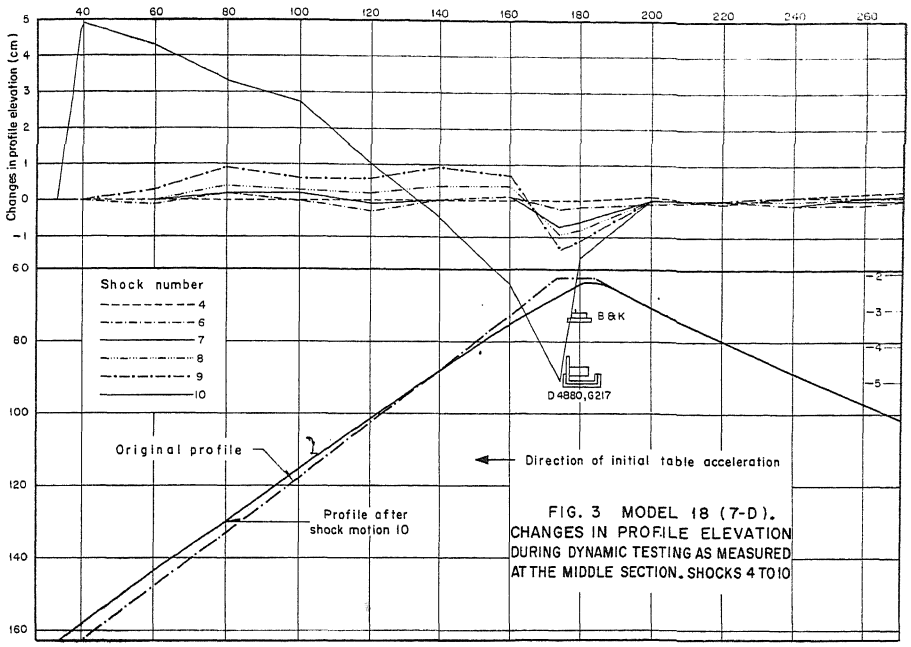

FIG. 3 MODEL 18 (7-D). CHANGES IN PROFILE ELEVATION DURING DYNAMIC TESTING AS MEASURED AT THE MIDDLE SECTION. SHOCKS 4 TO 10

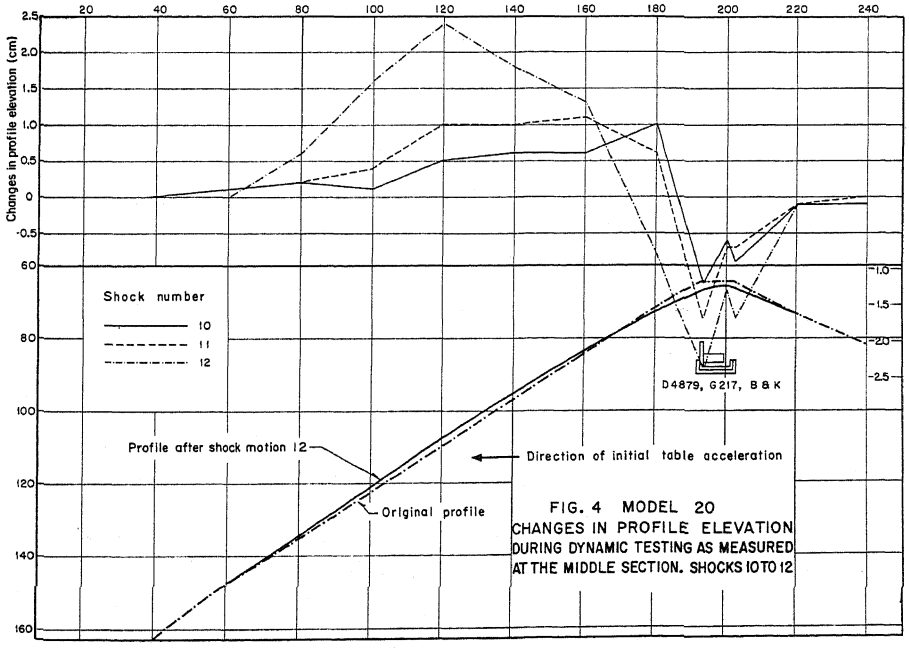

FIG. 4 MODEL 20 CHANGES IN PROFILE ELEVATION DURING DYNAMIC TESTING AS MEASURED AT THE MIDDLE SECTION. SHOCKS 10 TO 12

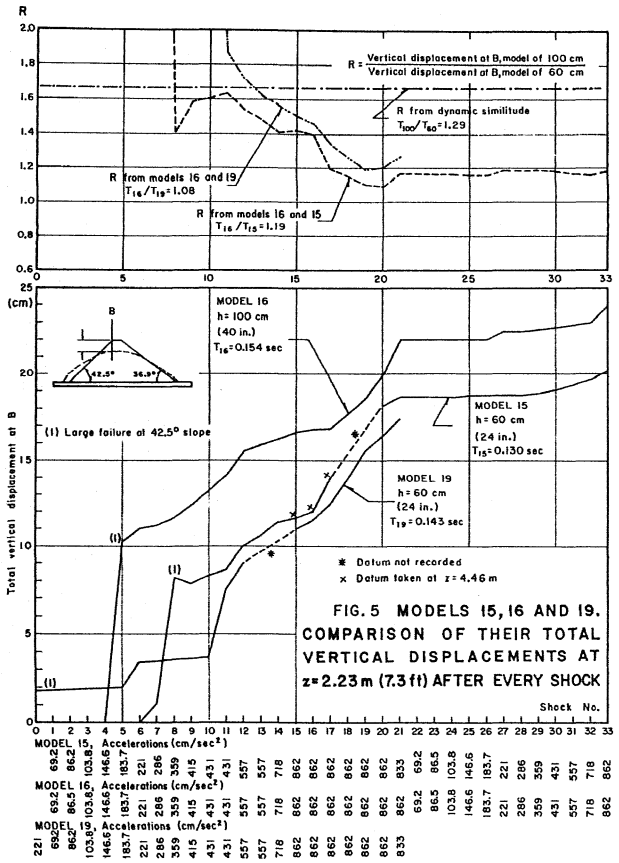

FIG. 5 MODELS 15, 16 AND 19. COMPARISON OF THEIR TOTAL VERTICAL DISPLACEMENTS AT z = 2.23 m (7.3 ft) AFTER EVERY SHOCK

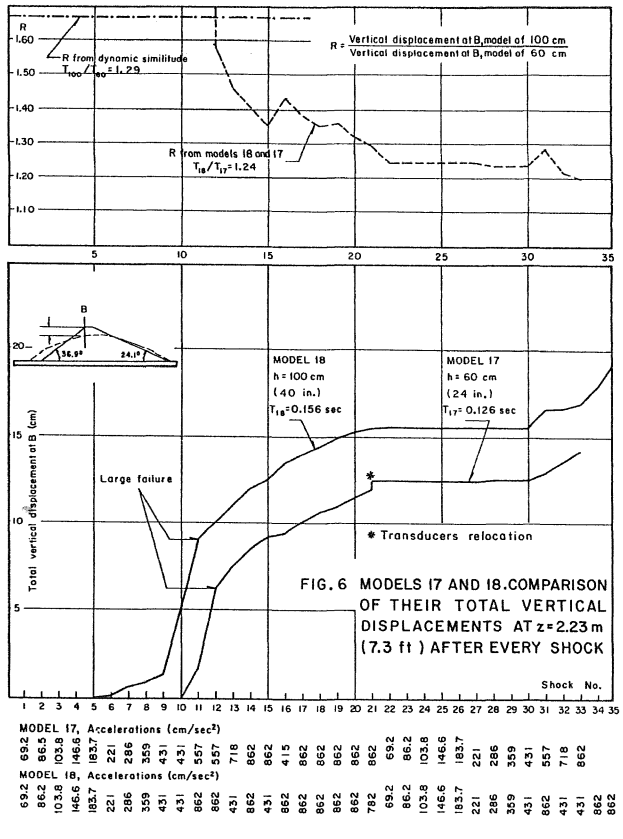

FIG. 6 MODELS 17 AND 18. COMPARISON OF THEIR TOTAL VERTICAL DISPLACEMENTS AT z = 2.23 m (7.3 ft) AFTER EVERY SHOCK

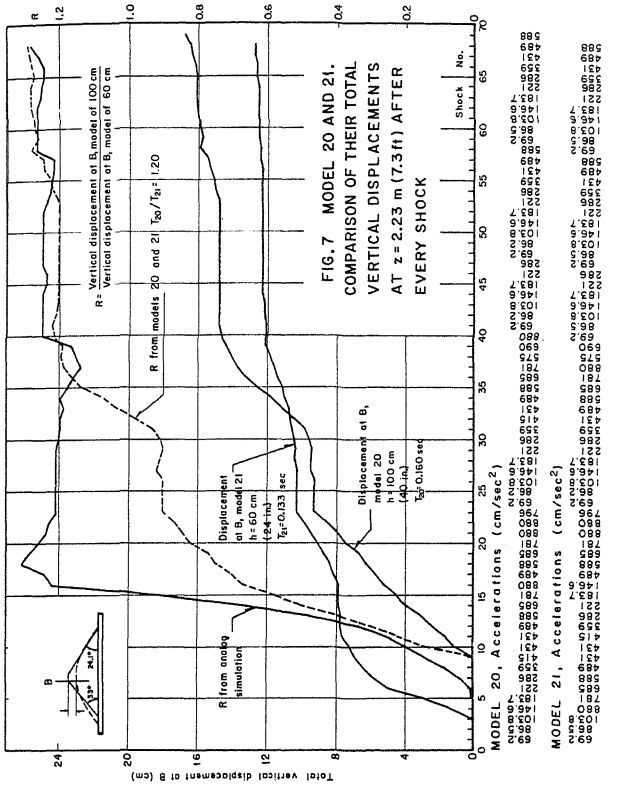

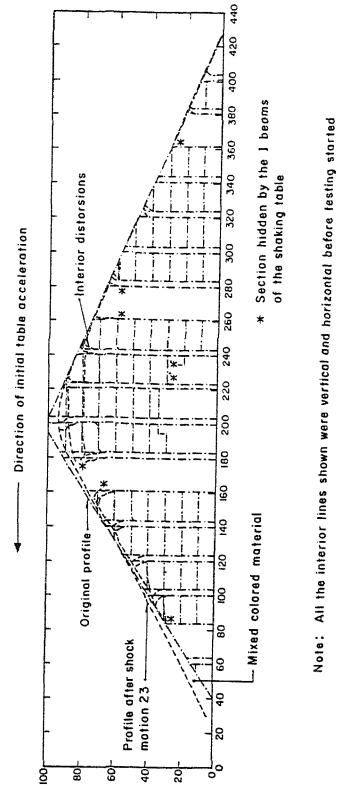

Note: All the interior lines shown were vertical and horizontal before testing started

FIG. 8 MODEL 20. PROFILE AND INTERIOR CHANGES DURING DYNAMIC TESTING UP TO SHOCK 23, AS OBSERVED AT THE NORTH PLEXIGLASS WALL

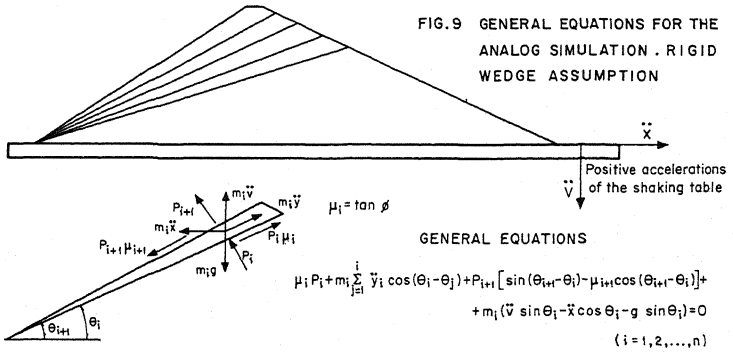

FIG. 9 GENERAL EQUATIONS FOR THE ANALOG SIMULATION. RIGID WEDGE ASSUMPTION

$\mu_i = \tan \phi$

GENERAL EQUATIONS

$$\mu_i P_i + m_i \sum_{j=1}^{i} \ddot{y}_i \cos(\theta_i - \theta_j) + P_{i+1}\left[\sin(\theta_{i+1} - \theta_i) - \mu_{i+1}\cos(\theta_{i+1} - \theta_i)\right] + m_i(\ddot{v}\sin\theta_i - \ddot{x}\cos\theta_i - g\sin\theta_i) = 0 \quad (i = 1, 2, \ldots, n)$$

$$P_i - m_i \sum_{j=1}^{i} \ddot{y}_i \sin(\theta_i - \theta_j) - P_{i+1}\left[\cos(\theta_{i+1} - \theta_i) + \mu_{i+1}\sin(\theta_{i+1} - \theta_i)\right] + m_i(\ddot{v}\cos\theta_i + \ddot{x}\sin\theta_i - g\cos\theta_i) = 0 \quad (i = 1, 2, \ldots, n)$$

CONDITIONS

1. $P_{n+1}(t) = 0$, Fixed boundary condition.
2. $\ddot{y}_k(t) = \dot{y}_k(t) = 0$, Moving boundary condition. (k = the lowest wedge that does not move relatively to the shaking table at time t)
3. $P_i > 0, (i = 1, 2, \ldots, n)$
4. $\mu_i = +\tan\phi$, if $\dot{y}_i - \dot{y}_{i-1}\cos(\theta_i - \theta_{i-1}) > 0$; $\mu_i = -\tan\phi$, if $\dot{y}_i - \dot{y}_{i-1}\cos(\theta_i - \theta_{i-1}) < 0$; $|\mu_i| \leq \tan\phi$, if $\dot{y}_i - \dot{y}_{i-1}\cos(\theta_i - \theta_{i-1}) = 0$

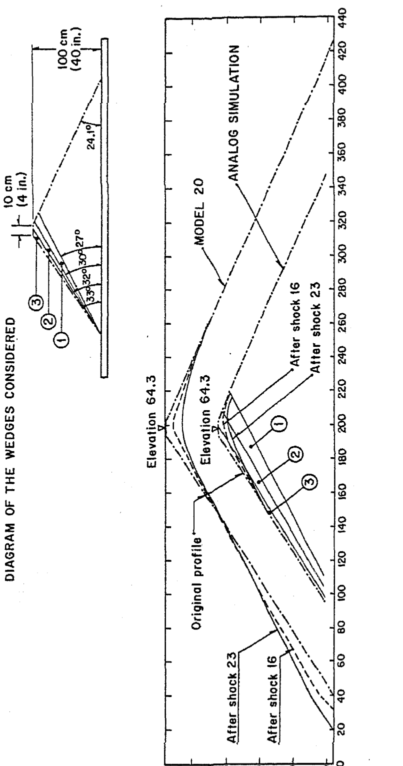

FIG. 10 COMPARISON OF THE PROFILE FROM MODEL 20 AND FROM THE ANALOG SIMULATION OF IT

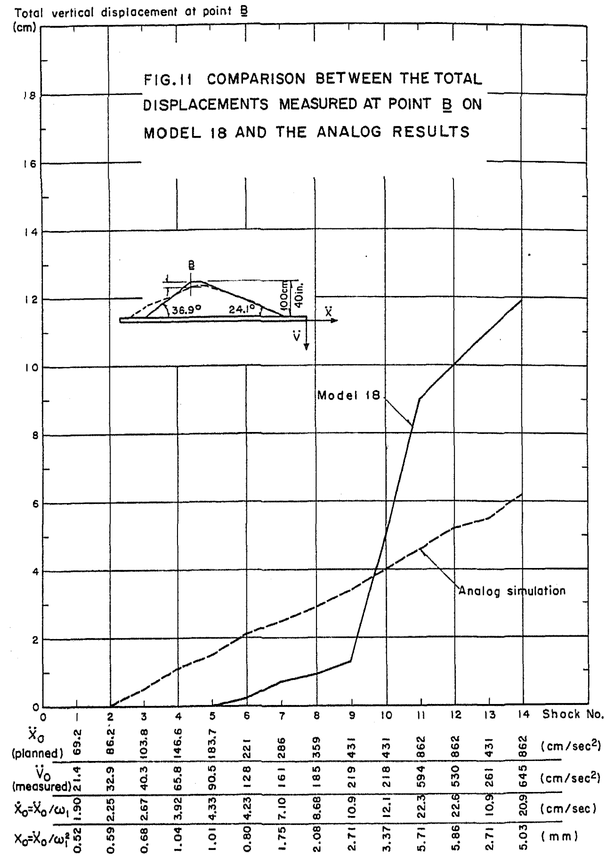

FIG. 11 COMPARISON BETWEEN THE TOTAL DISPLACEMENTS MEASURED AT POINT B ON MODEL 18 AND THE ANALOG RESULTS

Shock No.	1	2	3	4	5	6	7	8	9	10	11	12	13	14	
$\ddot{X}_0$ (planned)	69.2	86.2	103.8	146.6	183.7	221	286	359	431	431	862	862	431	862	(cm/sec²)
$\ddot{V}_0$ (measured)	21.4	32.9	40.3	65.8	90.5	128	161	185	219	218	594	530	261	645	(cm/sec²)
$\dot{X}_0=\ddot{X}_0/\omega_1$	1.90	2.25	2.67	3.92	4.33	4.23	7.10	8.68	10.9	12.1	22.3	22.6	10.9	20.9	(cm/sec)
$X_0=\ddot{X}_0/\omega_1^2$	0.52	0.59	0.68	1.04	1.01	0.80	1.75	2.08	2.71	3.37	5.71	5.86	2.71	5.03	(mm)

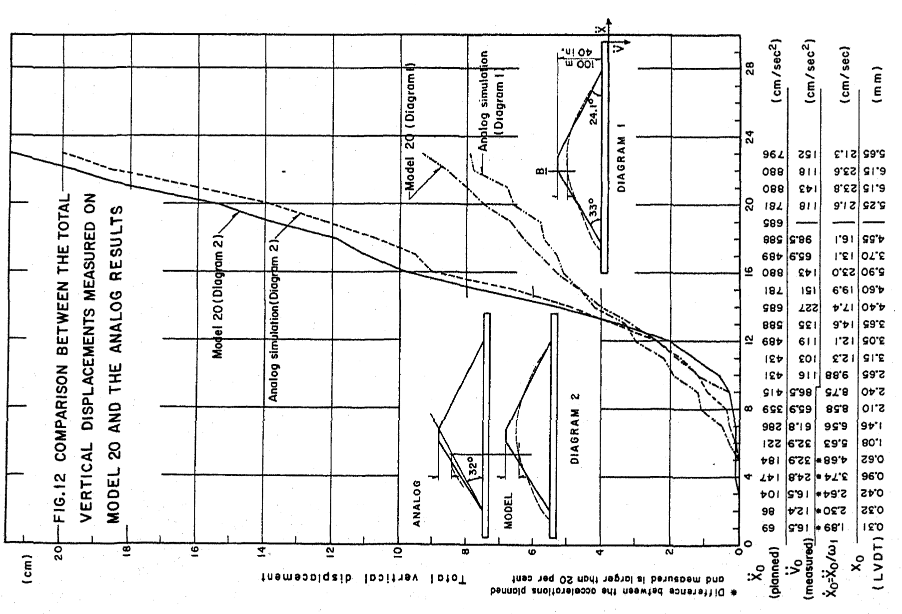

FIG. 12 COMPARISON BETWEEN THE TOTAL VERTICAL DISPLACEMENTS MEASURED ON MODEL 20 AND THE ANALOG RESULTS